JAERI 1111

JAERI 1111

Method for Measuring Void Fraction by Electromagnetic Flowmeters

August 1966

日 本 原 子 力 研 究 所

Japan Atomic Energy Research Institute

日本原子力研究所は，研究成果，調査結果の報告のため，つぎの3種の研究報告書を，それぞれの通しナンバーを付して，不定期に公刊しております．

1. 研究報告	まとまった研究の成果あるいはその一部における重要な結果の報告	JAERI 1001-3999
2. 調査報告	総説，展望，紹介などを含め，研究の成果，調査の結果をまとめたもの	JAERI 4001-5999
3. 資　　料	研究成果の普及，開発状況の紹介，施設共同利用の手引など	JAERI 6001-6999

このうち既刊分については「JAERI レポート一覧」にタイトル・要旨をまとめて掲載し，また新刊レポートは「原研びぶりお」でその都度紹介しています．これらの研究報告書に関する頒布，版権，複写のお問合せは，日本原子力研究所技術情報部（茨城県那珂郡東海村）あてお申し越しください．

Japan Atomic Energy Research Institute publishes the nonperiodical reports with the following classification numbers:

1. **JAERI** 1001-3999 Research reports,
2. **JAERI** 4001-5999 Survey reports and reviews,
3. **JAERI** 6001-6999 Information and Guiding Booklets.

Any inquiries concerning distribution copyright and reprint of the above reports should be derected to the Division of Technical Information, Japan Atomic Energy Research Institute, Tokai-mura, Naka-gun, Ibaraki-ken, Japan.

編集兼発行　日本原子力研究所

JAERI 1111 UDC 532.57.082.7 : 532.529

Method for Measuring Void Fraction by Electromagnetic Flowmeters

Summary

The electromagnetic void meter has been developed for the studies of gas-liquid two-phase flows. Calibration experiments have been completed, using argon-mercury and air-water two-phase flows through a pipe. The results show that this method can be used for two-phase flows with a non-oscillatory flow pattern (bubble flow) without calibration, and with calibration for the oscillatory flow pattern (slug flow). This method may be applicable to two-phase flows in more complex shaped channels and in boiling conditions.

August, 1966

MASAO HORI
TETSUO KOBORI
YOSHIHIRO OUCHI
Division of Power Reactor Development
Tokai Research Establishment, Japan Atomic Energy Research Institute

電磁流量計によるボイド体積率計測

要　旨

気液二相流のボイド体積率を計測する手段として，電磁流量計による方法を開発し，アルゴン—水銀および空気—水二相流で検定実験をおこない，気泡液やスラッグ流などの二相流々動状態について，充分な精度で測定できることを実証した．

この方法は電磁流量計の出力が電気伝導性をもった流体の流速，すなわち気液二相流の場合には，液体の流速のみに比例することを利用したものであって，複雑な流路にも適用できる．

1966年8月

日本原子力研究所　東海研究所
動力炉開発部　堀　雅夫
小堀哲雄
大内義弘

Contents

目　次

1. Introduction

In a boiling water reactor, the void fraction in the steam-water two-phase flow system is very important because the void fraction has an effect on the reactivity of the reactor. The void fraction is also important for calculating the recirculation flow rate in a natural circulation system. To obtain the data for the design and analysis of boiling reactors, various types of void measuring methods have been devised.

The electromagnetic void meter reported here is one of these method. The principle—measuring the average velocity of the liquid phase—is the same as the turbine flowmeter.

Calibration experiments were made using argon-mercury[1] and air-water two-phase flows[2]. Simulated void experiments were also made for investigating the void pattern.

Results of these calibration experiments showed that this electromagnetic method was applicable to void fraction measurement for the two-phase bubble flow without calibration.

The outputs of the electromagnetic flowmeter through which the liquid and gas flowed in various mixing ratios, were recorded with an oscillograph. It was considered that these outputs recordings could be used in the estimation of two-phase flow pattern for opaque liquids.

2. Void measuring method

Electromagnetic flowmeters are usually used to measure the velocity of a conducting fluid. When the fluid flows through a pipe as in **Fig. 1**, the electromotive force acting in the direction

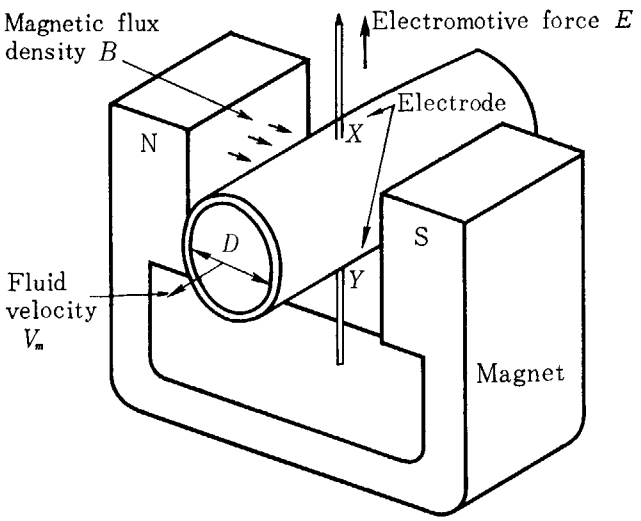

Fig. 1 Transverse-field type electromagnetic-flowmeter

perpendicular both to the motion and to the magnetic field is as follows:

$$E=KDBV_m\times 10^{-3} \qquad (1)$$

where E is the electric potential difference (mV) between the two electrodes X and Y, D is the distance (cm) XY which is equal to the pipe diameter, B is the effective value (gauss) of the magnetic flux density applied, V_m is the mean flow velocity (m/sec), and K is a measure of the performance or calibration of any transverse-field type flowmeter. If the pipe wall is made of an insulating material and the velocity profile is axisymmetric, K is independent of the velocity distribution and is equal to unity[3].

If, as shown in **Fig. 2** (I), the electromagnetic flowmeter (II) is set to the pipe through which the gas and conducting liquid flow, the gas in the dispersed phase and the liquid in the continuous phase, the electromotive force corresponding to the average velocity, V_{II}, of the liquid phase can be measured. When the volumetric flow rate Q_{II}, is known, the cross-sectional area, A_1, through which the liquid phase flows, is calculated from the equation :

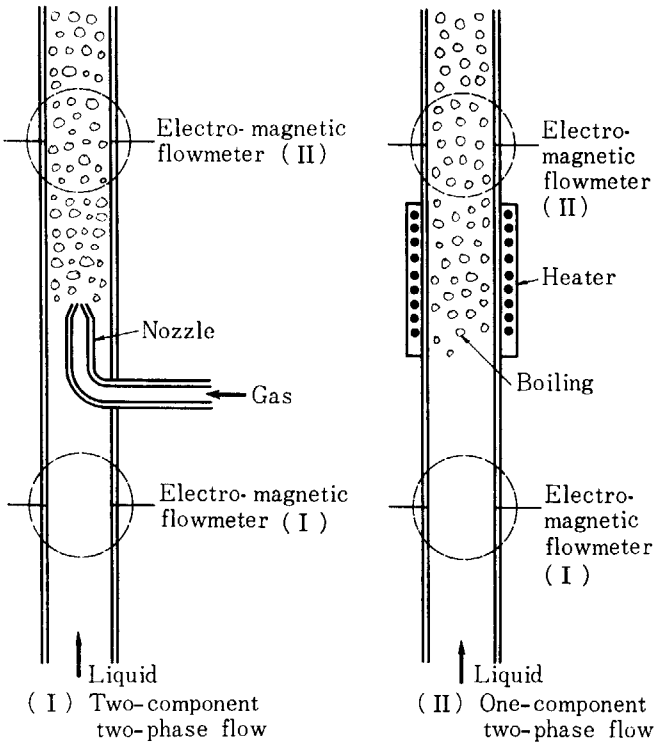

Fig. 2. Void fraction measurement using two electromagnetic-flowmeter

$$A_1 = Q_{II}/V_{II} \tag{2}$$

Thus the void fraction α is obtained as follows :

$$\alpha = (A_P - A_1)/A_P = 1 - Q_{II}/A_P V_{II} \tag{3}$$

where A_P is the total cross-sectional area of the pipe. If another flowmeter (I) is used to measure the liquid flow rate, Q_I, as shown in **Fig. 2** (I), the void fraction is calculated from Eq. (4) using the electromotive forces of the two flowmeters,because Q_I, is equal to Q_{II}.

$$\alpha = 1 - K_{II}D_I B_{II}E_I/K_I D_{II}B_I E_{II} = 1 - K(E_I/E_{II}) \tag{4}$$

If the two flowmeters are of the same specifications and the velocity profile is axisymmetric in the both flowmeters, $K_I B_I/D_I$ is equal to $K_{II}B_{II}/D_{II}$ i. e. $K=1$, and Eq. (5) is obtained.

$$\alpha = 1 - (E_I/E_{II}) \tag{5}$$

In **Fig. 2** (I) are shown the measurements for a liquid into which gas or vapor bubbles are introduced and in which there is no change in phase between the flowmeter (I) and (II) in the case of two-component two-phase flow. **Fig. 2** (II) shows the case of a one-component two-phase flow with phase change between two flowmeters. In the latter case, the void fraction is given by Eq. (6), because Q_{II} is equal to $Q_I(1-x)$.

$$\alpha = 1 - KE_I(1-x)/E_{II} \tag{6}$$

where x is the quality of the two-phase flow at the flowmeter (II). For introducing Eqs. (4) and (5), it is assumed that Q_{II} or $Q_{II}(1-x)$ is always equal to Q_I. This means that the void fraction at the flowmeter (II) does not vary with time. In the case of a two-phase flow pattern of bubble flow, this postulation is true. In slug flow, however, the void fraction changes in the manner of oscillation and Q_{II} or $Q_{II}(1-x)$ is not always equal to Q_I. Therefore Eqs.

(4) and (5) do not hold exactly. This problem will be discussed in Chapter 5.

In the actual measurements of void fractions, direct-current type electromagnetic flowmeters are used for liquid metal two-phase flows, and alternating-current type electromagnetic flowmeters for air water two-phase flows. For the measurements of the flow velocity of water, direct-current type flowmeters can not be used because of the electrolytic polarization on the electrodes.

3. Feasibility studies with mercury

3.1 Experimental Apparatus

The experimental apparatus used for feasibility studies is shown in **Fig. 3**. This apparatus was originally constructed to investigate the characteristic of circulation of mercury by the gas-lift principle. In this experiment, mercury was also used as the conducting liquid.

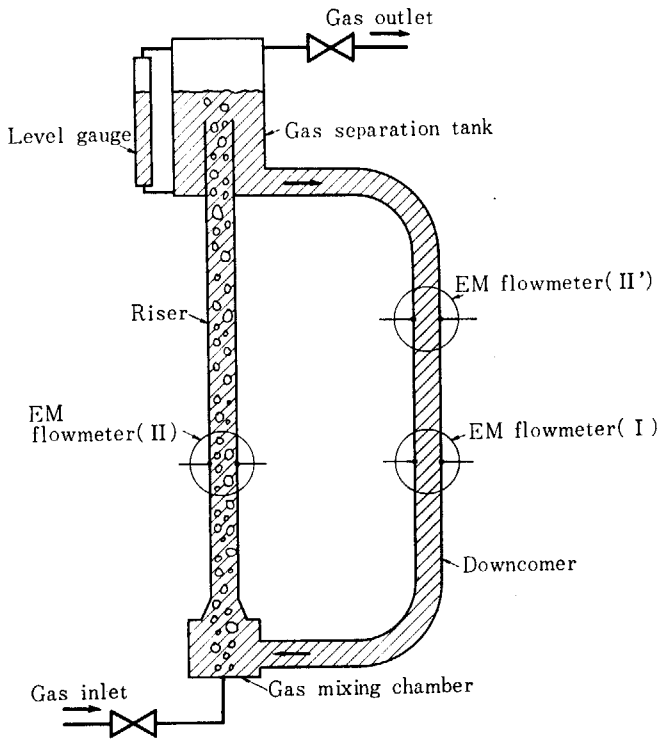

Fig. 3 Experimental apparatus of argon-mercury calibration

Argon gas is injected through a nozzle into the gas mixing chamber to produce gas bubbles in the mercury in the riser. Mercury is circulated through the loop, due to the difference in the density between the riser and downcomer. The gas is separated from the mercury in a gas separation tank and is exhausted into the atmosphere. Only mercury goes through the downcomer.

The inside diameter of the downcomer is 28.0 mm. The dimensions of the riser can be changed as follows :

Inside diameter : 27.8, 21.1, 15.7, 13.0 mm
Riser height : 200, 150, 100 cm

Two direct-current electromagnetic flowmeters with permanent magnets were used ; the flux densities were about 1600 gausses, and the diameters of the pole faces were 38 mm. The material of the pipe wall of the flowmeter was an acrylic resin with no electric conductivity, and the copper rods (diameter : 5 mm) were attached on the pipe wall as the electrodes.

In order to avoid the cut-off of the output signal from the flowmeters, due to covering of the electrode with gas bubbles, copper which is wetted fairly well by mercury was chosen for the electrodes.

3. 2 Simulated void calibration

First, calibration experiments were made with simulated voids of glass rod to investigate the effects of the void pattern and the orientations of the voids. Two flowmeters (I) and (II) were set to the pipe of the downcomer as shown in **Fig. 3**. The flowmeter (I) was used to measure the flow rate of mercury and the flowmeter (II) to measure the velocity flowing through the pipe with simulated voids. The different sets of glass rods as shown in **Fig. 4**

TABLE 1 Dimension of simulated void

void No.	Diameter of glass rod d (mm)	Number of glass rod N	Pitch p (mm)	Eccentricity ε (mm)	Void area A_V (cm²)	Void fraction α_{CR} (%)
MS- 1	7. 4	1		0	0. 431	7. 21
MS- 2	{ 8. 1 6. 85	2	11. 4	0	0. 884	14. 77
MS- 3	〃	〃	〃	90° rotated	〃	〃
MS- 4	4. 14±0. 40	9	7. 0	0	1. 215	20. 3
MS- 5	5. 59±0. 16	5	7. 2	0	1. 229	20. 5
MS- 6	〃	〃	〃	90° rotated	〃	〃
MS- 7	7. 73±0. 27	3	9. 7	0	1. 409	23. 6
MS- 8	〃	〃	〃	90° rotated	〃	〃
MS- 9	15. 5	1		0	1. 884	31. 5
MS-10	〃	〃		3 mm to pole	〃	〃
MS-11	〃	〃		3 mm to electrode	〃	〃
MS-12	18. 35	1		0	2. 65	44. 2
MS-13	21. 0	1		0	3. 24	54. 1
MS-14	21. 7	1		0	3. 69	61. 6

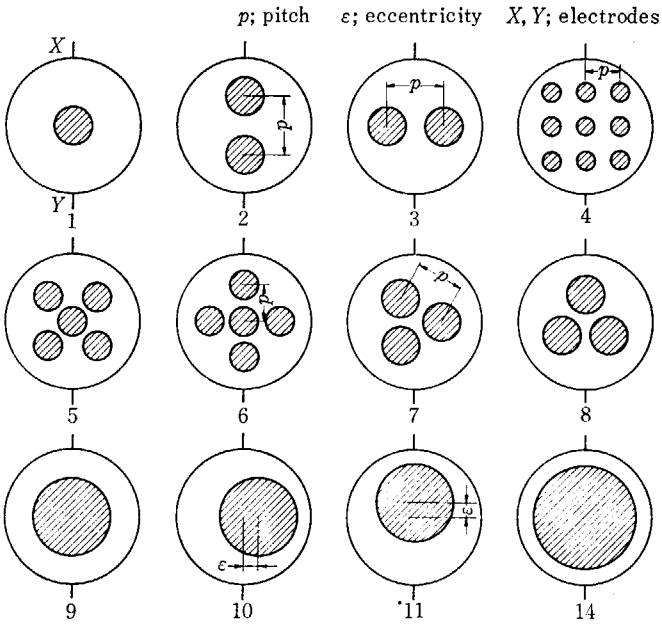

Fig. 4 Simulated void patterns

were inserted into the flowmeter (II'). The dimensions and the configurations of the simulated voids are given in TABLE 1. The void fraction defined as the ratio of the cross sectional area of the simulated voids to that of the pipe was changed from 7. 2 to 61. 6%. The velocity of mercury was changed from 0. 1 to 1. 0 m/sec. The effect of the eccentricity of the rod position was investigated for the one-rod pattern, and the effect of the orientation was investigated for the multi-rod void (2, 3, 5 rods) as shown in **Fig. 4**.

3. 2. 1 Magnetic flux

Prior to the calibration experiment, the magnetic fluxes of the flowmeter (I) and (II) were measured with a magnetic flux meter ; the measuring principle is the Hall effect (accuracy : ±3%). The local magnetic flux was measured every 1 mm in the directions normal and parallel to the pole face, and the average magnetic flux was calculated from these local values by integration.

Data obtained are plotted in **Figs. 5** and **6**. The magnetic flux distribution is similar to the surface of hyperbolic paraboloid ; the magnetic fluxes at the center are minimum and maximum, in the directions normal and parallel to the pole face, respectively.

The average magnetic flux of the flowmeter (I), B_{mI}, was 1773 gausses, and that of the flowmeter (II), B_{mII}, 1609 gausses. As the dimensions and configurations of the two flowmeters are the same, the ratio of the outputs from the flowmeters for same flow velocity is

$$(E_{II}/E_I)_0 = (K_{II}B_{mII}D_I/K_IB_{mI}D_{II}) = 0.907 \qquad (7)$$

The suffix 0 indicates the case without simulated voids in the flowmeter (II). To check this ratio, mercury was circulated through two flowmeters, with no glass rod in the flowmeter (II). The results obtained are presented in TABLE 2.

The agreement between the calculated and measured values of $(E_{II}/E_I)_0$ is fairly good. In the calibration experiment, measured value of $(E_{II}/E_I)_0$ in TABLE 2 was used for the correction factor in Eq. 8.

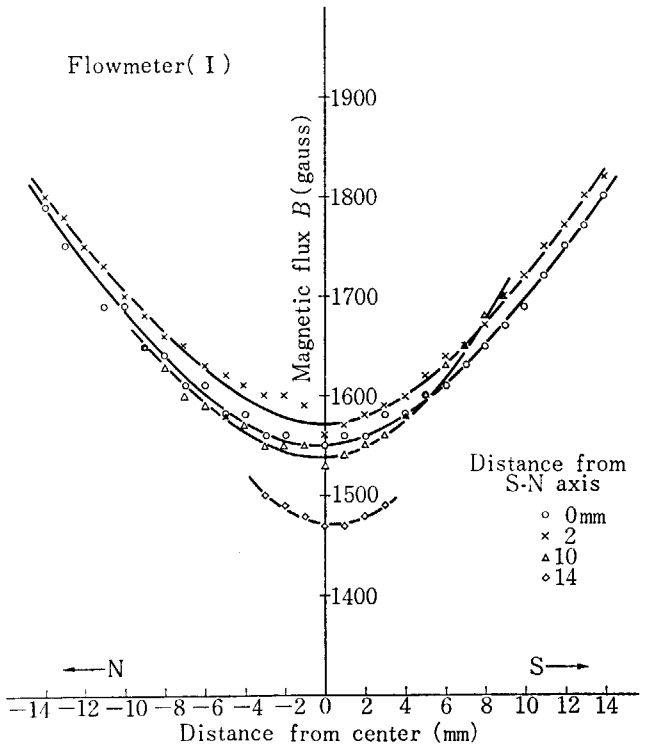

Fig. 5 Magnetic flux distribution : normal to pole face

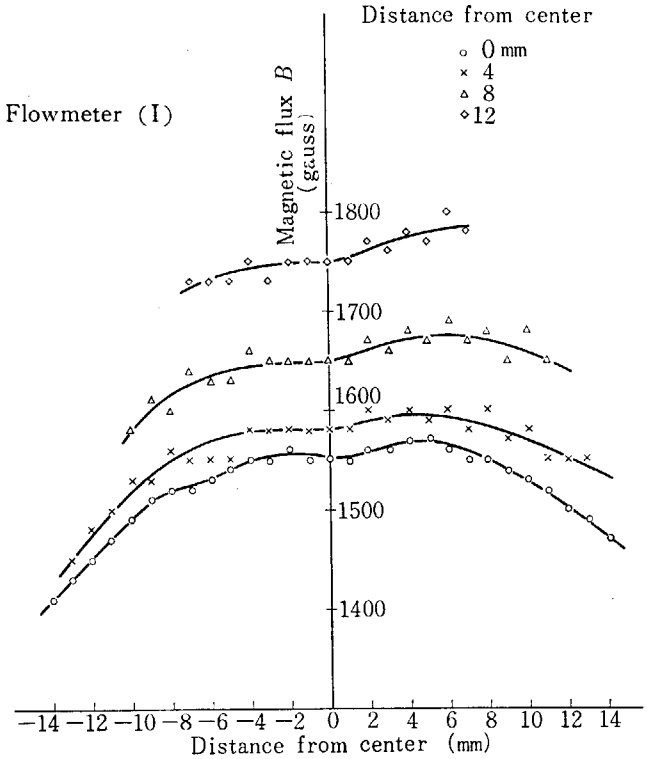

Fig. 6 Magnetic flux distribution : parallel to pole face

TABLE 2 Zero void experiment

No.	Output of flowmeter		$(E_{II}/E_I)_0$
	E_{I_0}	E_{II_0}	
1	0. 60 mV	0. 55 mV	0. 918
2	1. 10	0. 98	0. 898
3	1. 45	1. 32	0. 910
4	1. 63	1. 46	0. 896
5	1. 96	1. 78	0. 908
6	2. 27	2. 03	0. 894
7	2. 40	2. 16	0. 901
8	2. 55	2. 30	0. 903
9	2. 75	2. 47	0. 898
10	2. 85	2. 60	0. 900
11	2. 99	2. 69	0. 887
	Mean		0. 9005

$$\alpha_{EM}=1-K(E_I/E_{II}) \tag{8}$$

where

$$K=(E_{II}/E_I)_0$$

This correction factor K changes with time, due to the decrease in the magnetic flux of the flowmeter and so K was checked, each time just before the calibration experiment.

3. 2. 2 Calibration experiments

Data obtained with various types of simulated voids are presented in TABLE 3.

First, the effect of the liquid flow rate on the void fraction was investigated. The flow rate of mercury was changed from 100 to 410 cm^3/sec. The effect of the flow rate on the

TABLE 3 Experimental data (Simulated void)

Run No.	Liquid Velocity V_I (cm/sec)	Output of flowmeter E_I (mV)	Output of flowmeter E_{II} (mV)	E_I/E_{II}	Void Fraction $\alpha_{meas.}$ (%)	$\alpha_{meas.}/\alpha_{calc.}$
MS- 1-01	74.6	2.78	2.65	1.049	5.50	0.763
2	59.3	2.21	2.135	1.035	6.75	0.936
3	49.1	1.835	1.77	1.036	6.65	0.922
4	38.0	1.42	1.365	1.041	6.20	0.860
5	20.9	0.78	0.75	1.040	6.30	0.874
6	21.1	0.79	0.76	1.039	6.40	0.888
7	38.5	1.44	1.385	1.040	6.30	0.874
8	49.8	1.86	1.79	1.039	6.40	0.888
9	59.1	2.205	2.11	1.045	5.85	0.811
10	74.2	2.765	2.66	1.040	6.30	0.874
			Mean	1.040	6.27	0.871
MS- 2-01	78.4	2.69	2.77	0.971	12.50	0.8465
2	63.4	2.17	2.235	0.971	12.50	0.8465
3	52.7	1.805	1.86	0.9705	12.55	0.850
4	43.4	1.485	1.525	0.974	12.25	0.8295
5	24.4	0.835	0.865	0.9655	13.00	0.8805
6	24.2	0.825	0.850	0.9705	12.55	0.850
7	43.2	1.480	1.510	0.980	11.70	0.792
8	54.5	1.865	1.910	0.9765	12.00	0.8125
9	62.8	2.15	2.20	0.977	11.95	0.809
10	78.0	2.675	2.75	0.9725	12.40	0.8395
			Mean	0.973	12.35	0.836
MS- 3-01	73.9	2.53	2.68	0.944	15.05	1.019
2	58.6	2.005	2.145	0.9345	15.9	1.076
3	50.3	1.72	1.825	0.943	15.15	1.026
4	38.8	1.33	1.415	0.940	15.40	1.042
5	19.4	0.665	0.70	0.950	14.5	0.982
6	20.4	0.70	0.74	0.946	14.85	1.005
7	39.6	1.355	1.45	0.9345	15.9	1.076
8	50.1	1.715	1.83	0.937	15.7	1.063
9	59.0	2.02	2.16	0.935	15.85	1.073
10	73.5	2.515	2.675	0.9405	15.35	1.039
			Mean	0.940	15.40	1.042
MS- 4-01	59.4	1.90	2.135	0.890	19.9	0.981
2	46.9	1.50	1.69	0.8875	20.15	0.993
3	38.6	1.235	1.39	0.8885	20.05	0.988
4	28.2	0.90	1.01	0.891	19.8	0.976
5	28.2	0.90	1.01	0.891	19.8	0.976
6	39.7	1.265	1.415	0.894	19.55	0.963
7	47.1	1.505	1.70	0.8855	20.3	1.000
8	59.9	1.91	2.16	0.8845	20.4	1.005
			Mean	0.889	20.0	0.985
MS- 5-01	72.8	2.32	2.56	0.906	18.45	0.900
2	57.2	1.825	2.005	0.910	18.1	0.883
3	47.0	1.50	1.65	0.909	18.2	0.888
4	34.0	1.085	1.19	0.912	17.9	0.873

TABLE 3 (Continued)

Run No.	Liquid Velocity V_L(cm/sec)	Output of flowmeter E_I(mV)	Output of flowmeter E_{II} (mV)	E_I/E_{II}	Void Fraction $\sigma_{meas.}$(%)	$\alpha_{meas.}/\alpha_{calc.}$
MS- 5-05	34. 5	1. 10	1. 21	0. 909	18. 2	0. 888
6	47. 7	1. 52	1. 685	0. 902	18. 8	0. 917
7	57. 4	1. 83	2. 02	0. 906	18. 45	0. 900
8	73. 0	2. 33	2. 575	0. 905	18. 55	0. 905
			Mean	0. 907	18. 4	0. 898
MS- 6-01	71. 3	2. 27	2. 52	0. 901	18. 9	0. 922
2	56. 0	1. 785	1. 975	0. 904	18. 65	0. 911
3	46. 0	1. 465	1. 62	0. 9045	18. 6	0. 907
4	32. 5	1. 035	1. 15	0. 900	19. 0	0. 927
5	33. 2	1. 06	1. 18	0. 898	19. 2	0. 937
6	46. 6	1. 485	1. 635	0. 908	18. 3	0. 893
7	55. 8	1. 78	1. 97	0. 9035	18. 7	0. 912
8	71. 9	2. 29	2. 53	0. 905	18. 55	0. 905
			Mean	0. 902	18. 8	0. 917
MS- 7-01	53. 6	1. 64	1. 91	0. 8585	22. 75	0. 964
2	42. 0	1. 29	1. 51	0. 8545	23. 1	0. 979
3	35. 8	1. 10	1. 28	0. 8595	22. 65	0. 960
4	27. 0	0. 825	0. 970	0. 8505	23. 45	0. 994
5	27. 4	0. 840	0. 975	0. 8615	22. 5	0. 953
6	36. 5	1. 12	1. 29	0. 8685	21. 8	0. 924
7	43. 4	1. 33	1. 535	0. 8665	22. 0	0. 932
8	54. 4	1. 67	1. 94	0. 861	22. 55	0. 954
			Mean	0. 860	22. 6	0. 958
MS- 8-01	51. 1	1. 57	1. 82	0. 863	22. 3	0. 945
2	39. 8	1. 22	1. 425	0. 856	22. 95	0. 972
3	34. 3	1. 05	1. 22	0. 861	22. 5	0. 953
4	26. 1	0. 800	0. 920	0. 8695	21. 8	0. 924
5	26. 1	0. 800	0. 940	0. 851	23. 4	0. 992
6	34. 3	1. 05	1. 22	0. 861	22. 5	0. 953
7	40. 5	1. 24	1. 44	0. 861	22. 5	0. 953
8	51. 1	1. 57	1. 825	0. 8605	22. 55	0. 956
			Mean	0. 860	22. 6	0. 958
MS- 9-01	77. 3	2. 125	2. 73	0. 778	30. 0	0. 952
2	59. 3	1. 63	2. 10	0. 776	30. 15	0. 957
3	49. 4	1. 355	1. 74	0. 779	29. 9	0. 949
4	34. 6	0. 95	1. 24	0. 766	31. 05	0. 986
5	33. 8	0. 93	1. 20	0. 775	30. 25	0. 960
6	49. 9	1. 37	1. 755	0. 781	29. 7	0. 943
7	59. 8	1. 64	2. 10	0. 781	29. 7	0. 943
8	77. 0	2. 12	2. 73	0. 7765	30. 1	0. 955
			Mean	0. 777	30. 05	0. 954
MS-10-01	73. 6	2. 02	2. 615	0. 7725	30. 45	0. 966
2	57. 8	1. 585	2. 035	0. 779	29. 9	0. 949
3	44. 7	1. 225	1. 58	0. 7755	30. 2	0. 959
4	33. 8	0. 930	1. 22	0. 762	31. 4	0. 997
5	34. 1	0. 935	1. 23	0. 760	31. 6	1. 003

TABLE 3 (Continued)

Run No.	Liquid Velocity V_L (cm/sec)	Output of flowmeter E_I (mV)	Output of flowmeter E_{II} (mV)	E_I/E_{II}	Void Fraction $\alpha_{meas.}$ (%)	$\alpha_{meas.}/\alpha_{calc.}$
MS-10-06	48.9	1.34	1.74	0.770	30.7	0.975
7	58.3	1.60	2.06	0.7765	30.1	0.955
8	74.3	2.04	2.64	0.773	30.4	0.965
			Mean	0.771	30.6	0.971
MS-11-01	68.9	1.895	2.47	0.767	31.0	0.984
2	53.3	1.465	1.90	0.771	30.6	0.971
3	44.0	1.21	1.57	0.771	30.6	0.971
4	31.6	0.87	1.15	0.7565	31.9	1.013
5	31.4	0.865	1.13	0.7655	31.1	0.987
6	44.9	1.235	1.60	0.772	30.5	0.968
7	53.8	1.48	1.92	0.771	30.6	0.971
8	69.2	1.90	2.47	0.769	30.8	0.978
			Mean	0.768	30.9	0.981
MS-12-01	97.6	2.17	3.60	0.603	42.3	0.957
2	83.5	1.86	3.10	0.600	42.60	0.964
3	67.1	1.49	2.485	0.5995	42.65	0.965
4	59.1	1.315	2.20	0.5975	42.85	0.970
5	48.2	1.075	1.80	0.597	42.9	0.971
6	47.6	1.06	1.775	0.597	42.9	0.971
7	61.0	1.36	2.255	0.603	42.3	0.957
8	68.6	1.53	2.55	0.600	42.60	0.964
9	82.6	1.84	3.06	0.6015	42.5	0.962
10	97.9	2.18	3.615	0.603	42.3	0.957
			Mean	0.600	42.60	0.964
MS-13-01	103.0	1.88	3.79	0.496	52.95	0.979
2	84.8	1.55	3.12	0.497	52.9	0.978
3	72.5	1.325	2.665	0.497	52.9	0.978
4	61.0	1.11	2.24	0.4955	53.0	0.980
5	52.8	0.96	1.94	0.495	53.05	0.981
6	52.4	0.955	1.925	0.496	52.95	0.979
7	58.0	1.06	2.115	0.501	52.5	0.9705
8	73.2	1.335	2.67	0.500	52.6	0.972
9	85.9	1.57	3.15	0.4985	52.75	0.975
10	102.2	1.87	3.75	0.499	52.7	0.974
			Mean	0.499	52.7	0.974
MS-14-01	103.1	1.57	3.45	0.455	59.05	0.958
2	81.3	1.235	2.70	0.4575	58.8	0.954
3	68.3	1.04	2.265	0.459	58.7	0.953
4	51.8	0.785	1.70	0.462	58.4	0.948
5	51.4	0.78	1.71	0.456	58.05	0.942
6	67.0	1.02	2.225	0.4585	58.7	0.953
7	83.1	1.26	2.73	0.4615	58.55	0.950
8	104.5	1.59	3.45	0.461	58.5	0.950
			Mean	0.461	58.5	0.950

measured void fraction α_{EM} could not be observed as shown in **Fig. 7**. **Fig. 8** shows the magnitude of the scattering of the measured void fractions; dependency on the mercury flow velocity is not seen, except that the data are scattered more widely for low liquid velocities.

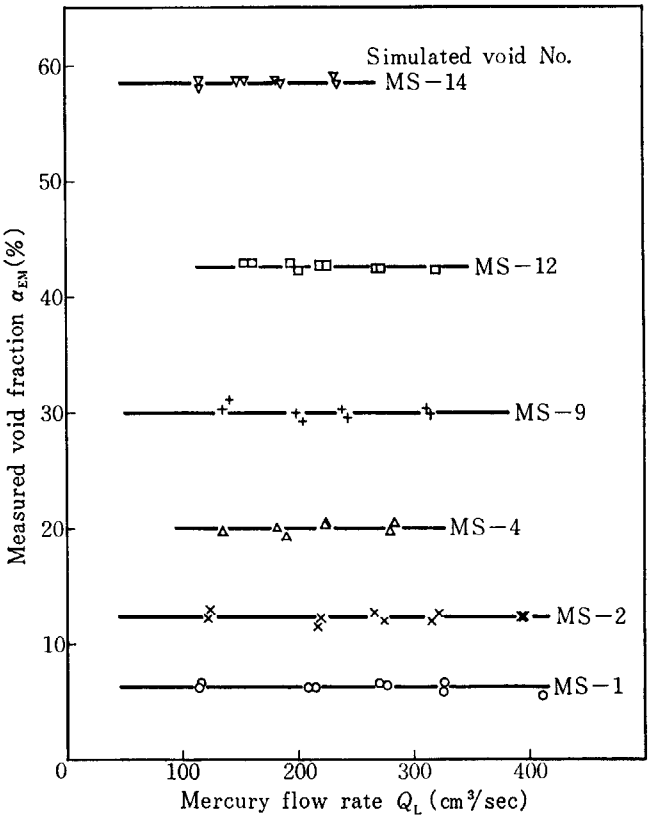

Fig. 7 Effect of mercury flow rate

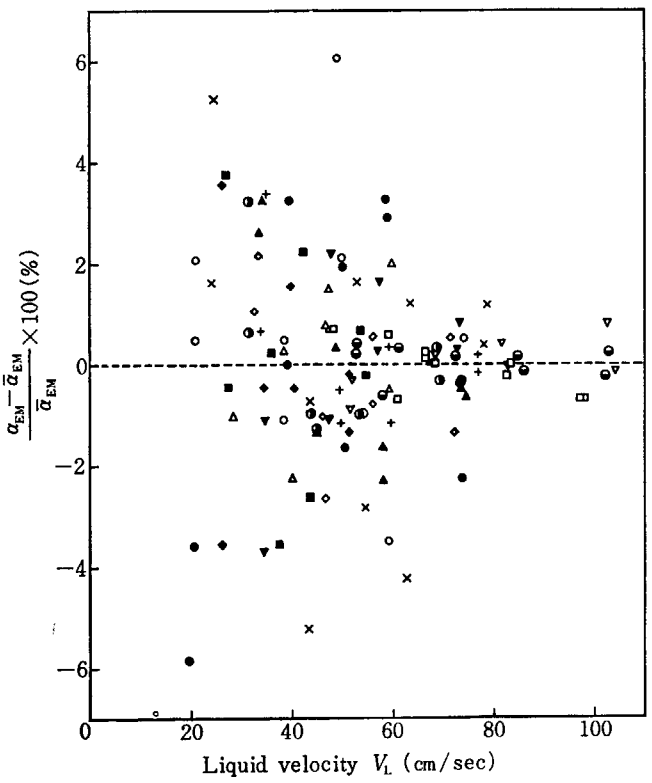

Fig. 8 Effect of liquid velocity on measured void fraction

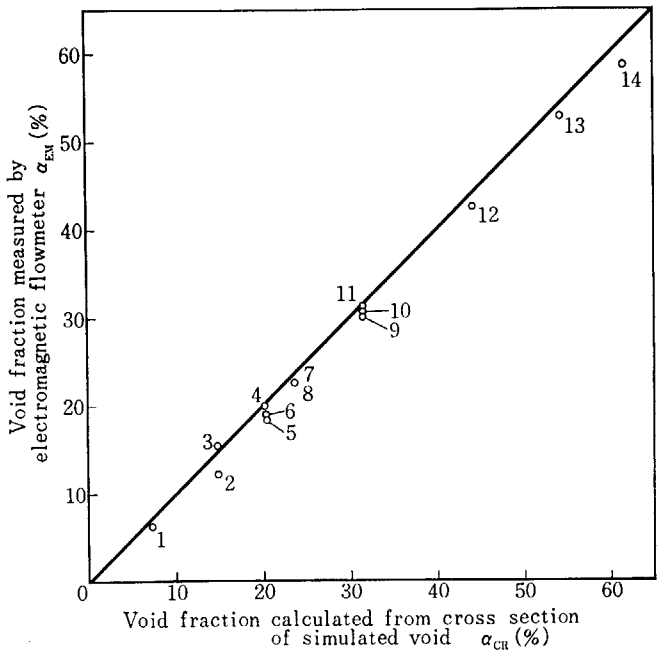

Fig. 9 Results of calibration experiment with simulated void

The average values for each simulated void are plotted in **Fig. 9** against the void fractions calculated from the cross sectional areas of simulated voids. Both values agree well, but there is a tendency that the void fraction measured is smaller than that calculated.

The effects of the void pattern, the eccentricity and the orientation were also investigated; nine different void patterns, three eccentricities and two different orientations. The variations of the void pattern, eccentricity and orientation may cause the change in the distribution of the liquid flow velocity and thus should produce a change in the outputs from the electromagnetic flowmeters. The experimental data do not show the clear dependency on these factors.

3. 3 Argon-mercury calibration

In the calibration for the void fraction in argon-mercury two-phase flows, the mercury circulating loop shown in **Fig. 3** was also used. Two electromagnetic flowmeters were set in the riser and downcomer. The specifications for the flowmeters (I) and (II) are given in

TABLE 4 Specifications of flowmeters

Specifications of flowmeters		Run Number			
		MR-11~MR-14	MR-21~MR-23	MR-31~MR-34	MR-41~MR-44
Riser	Inside diameter D_{II} mm	27. 8	21. 1	15. 7	13. 0
	Flow area A_{II} cm²	6. 05	3. 51	1. 95	1. 32
	Magnetic flux B_{II} gauss	1574	1576	1555	1550
	Pole face length/ Inside dia l_{II}/D_{II}	1. 369	1. 797	2. 415	2. 935
	End shunt loss K_{II}	0. 8964	0. 9541	0. 9847	0. 993
Downcomer	Inside diameter D_I mm	28. 0			
	Flow area A_I cm²	6. 18			
	Magnetic flux B_I gauss	1667			
	Pole face length/ Inside dia l_I/D_I	1. 356			
	End shunt loss K_I	0. 8964			
Output correction factor		0. 953	1. 333	1. 825	2. 229

TABLE 4. The diameter of the riser was changed from 13.0 to 27.8 mm. The magnets used were the same as those used in the simulated void experiment. The void fraction was obtained from Eq. 8, and the correction factor K was checked by using the magnetic flux meter.

3.3.1 Argon-mercury two-phase flow phenomena

Gas bubbles in mercury tend to attach to the pipe wall, depending on circumstances, due to the poor wettability of mercury for the pipe wall. Covering an electrode with attached bubbles causes a cut-off of the flowmeter. In this chapter, the problem of cut-off of the output is discussed.

According to our other experiments on the mercury-gas two-phase flow, the flow pattern in these calibration experiments was probably in the region of the bubble flow or the bubbleslug flow ; argon gas injected into mercury goes through the riser in the form of small bubbles or of lumps of bubbles. Since the inside state of flow can not be observed on account of the opacity of mercury, the flow pattern mentioned above is only the supposition from the observation of the flow at the pipe wall. The inner surface of the pipe wall was observed and the behaviour of bubbles attached on the surface was investigated. The bubbles are divided into three classes ;

(1) Stationary bubbles……Bubbles are almost fixed and their adhension diameters are less than 1 mm.

(2) Flowing bubbles……Bubbles move along the surface more slowly than mercury. Their diameters are 1～4 mm.

(3) Momently attached bubbles……Bubbles which are probably separated from the lumps of bubbles in the core zone of the flow move and adhere momently to the surface of the pipe wall. Their diameters are greater than 4 mm.

Most of the attached bubbles were stationary bubbles and the momently attached bubbles were very few ; bubbles greater than 5 mm were observed only in the case of higher void fractions. Since only the bubbles which are greater than the diameter of the electrode (5 mm) affect the output of the flowmeter, the cut-off of the output can not occur so frequently. The momently attached bubble stay on the electrode for a very short time, so that the time of cut-off must be very short.

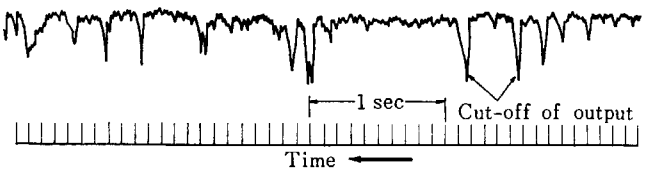

Fig. 10 Output of riser flowmeter

Fig. 10 shows the output of the riser flow meter which was recorded with an electromagnetic oscillograph. Owing to the fast response of the oscillograph, even very short cut-offs were recorded. When a bubble covers an electrode, the output circuit of the flowmeter is cut off and the output signal is lost, in consequence, the indication of the oscillograph goes steeply to zero. But it goes back to normal level halfway, since the bubble stays on the electrode too short a period for the indication to go to zero. This tendency becomes more remarkable for the recorder whose response is slower.

Figs. 11, 12, 13, 14 show the outputs of the flowmeters of the riser and the downcomer. They were recorded by an electronic potentiometer type mV recorder whose response time is 1/4 sec for full scale travelling. From these figures, the following facts were made clear.

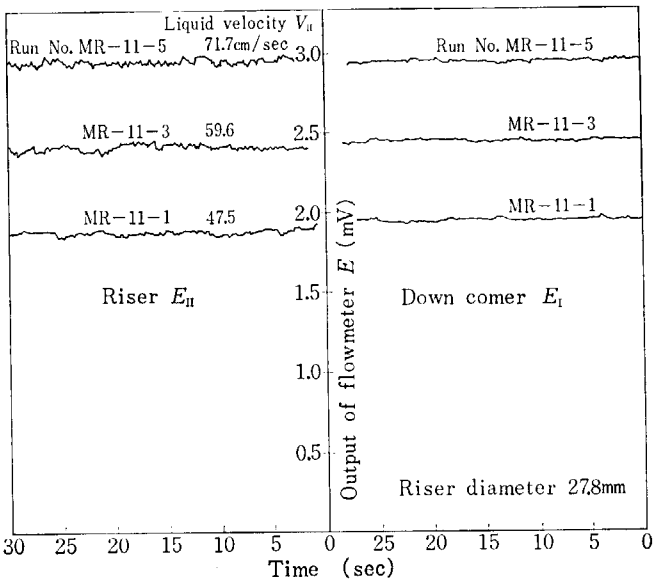

Fig. 11 Outputs of flowmeter (Riser diameter ; 27. 8 mm)

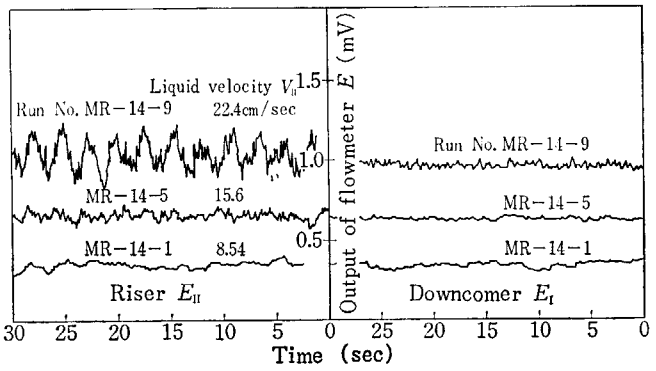

Fig. 12 Outputs of flowmeter (Riser diameter ; 27. 8 mm)

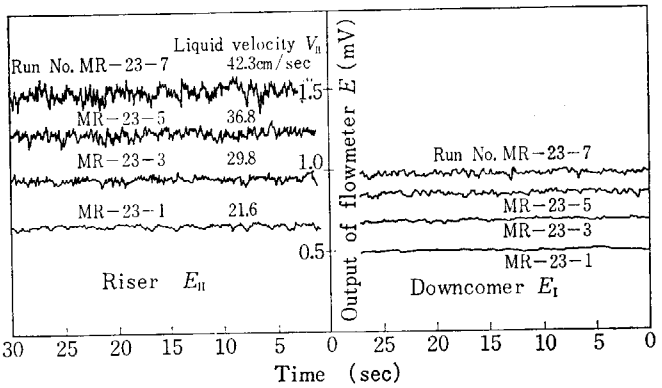

Fig. 13 Outputs of flowmeter (Riser diameter : 21. 1 mm)

While the void fraction is small or the velocity of mercury is large, in other words, as long as the flow pattern of the two-phase flow is the bubble flow, the probability that the bubble covers the electrode is quite small and the cut-off of the output scarcely occurs.

As the void fraction becomes large, the probability of the cut-off increases. But these fast and short signals can not be followed by the mV recorder and the normal value of the output can be recorded.

In conclusion, this type of void-meter can be used in the region of the bubble or bubble-slug flow without the serious obstruction from the attached bubbles.

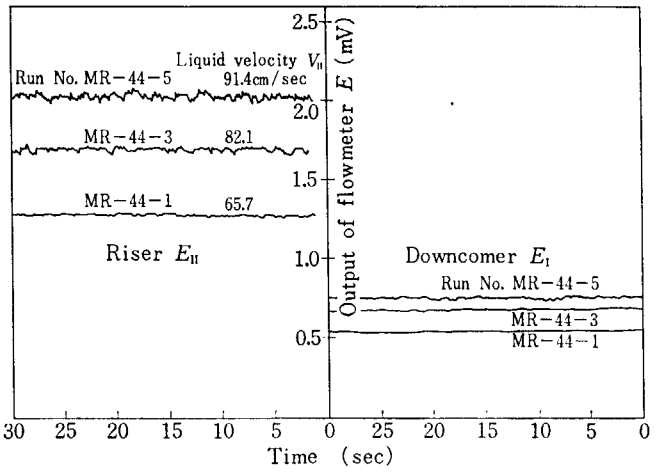

Fig.14 Outputs of flowmeter (Riser diameter ; 13. 0 mm)

3. 3. 2 Calibration results

The whole data taken with the real void are presented in TABLE 5. In this table, V_{IIS} is the superficial velocity of mercury which is supposed to flow filling the pipe of the riser, α_{LV} is the the void fraction obtained from the increase of the liquid level in the separation tank. Because the increase of the mercury level in the separation tank is proportional to the total volume of the ges in the riser, the average void fraction in the riser is calculated from Eq. 9.

TABLE 5 Experimental data (Real void)

Run No.	Liquid flow rate Q_L cm³/sec	Liquid velocity V_{II_5} (cm/sec)	Void fraction α_{LV}(%)	Void fraction α_{EM}(%)
MR-11-1	288	47. 5	2. 09	1. 18
2	317	52. 4	2. 76	2. 23
3	362	59. 6	3. 30	2. 99
4	396	65. 4	4. 03	3. 66
5	434	71. 7	4. 98	4. 90
6	476	78. 7	6. 07	6. 61
MR-12-1	237	39. 2	2. 44	2. 04
2	265	43. 8	3. 18	2. 42
3	296	48. 9	4. 07	3. 75
4	328	54. 2	5. 16	4. 99
5	355	58. 7	6. 18	6. 13
6	385	63. 6	6. 94	7. 95
MR-13-1	79. 2	13. 9	0. 872	1. 66
2	110	18. 2	1. 76	2. 00
3	133	21. 9	2. 83	4. 23
4	149	24. 6	3. 72	5. 66
5	174	28. 8	4. 56	5. 18
6	198	32. 8	6. 35	7. 18
7	217	35. 9	7. 63	8. 14
8	240	39. 6	9. 79	9. 47
9	258	42. 6	11. 3	11. 1
MR-14-1	51. 6	8. 54	1. 87	3. 37
2	58. 2	9. 63	2. 34	1. 99
MR-14-3	71. 5	11. 8	3. 69	5. 75
4	86. 2	14. 3	5. 19	5. 55
5	94. 4	15. 6	6. 24	6. 10
6	108	17. 9	8. 64	6. 61
7	119	19. 7	10. 9	9. 28
8	130	21. 4	12. 5	9. 00
9	136	22. 4	16. 2	16. 5
MR-21-1	302	86. 0	2. 87	2. 17
2	323	92. 1	3. 58	3. 87
3	346	98. 4	3. 91	5. 11
4	368	105	5. 16	7. 13
MR-22-1	143	40. 8	2. 54	2. 24
2	158	45. 1	3. 08	2. 57
3	182	51. 8	4. 46	4. 03
4	203	57. 9	5. 97	6. 18
5	223	63. 4	7. 19	7. 70
6	242	68. 8	8. 53	9. 93
7	259	73. 8	10. 3	11. 7
MR-23-1	75. 7	21. 6	3. 60	1. 55
2	84. 9	24. 2	5. 00	4. 67
3	105	29. 8	7. 63	5. 13
4	115	32. 9	9. 85	8. 81
5	129	36. 8	13. 2	10. 6

5 (Continved)

Run No.	Liquid flow rate Q_L cm³/sec	Liquid Velocity V_{IIs} (cm/sec)	Void fraction α_{LV}(%)	Void fraction α_{EM}(%)
MR-23-6	139	39.6	15.5	12.5
7	148	42.3	18.3	14.5
MR-31-1	175	90.0	2.71	1.53
2	192	98.6	3.40	3.36
3	205	105.4	5.60	5.52
4	215	110.7	8.22	8.28
5	223	114.9	8.54	11.0
MR-32-1	136	69.7	2.20	1.05
2	150	76.9	2.76	2.89
3	170	87.4	3.51	4.79
4	188	96.7	5.03	6.39
5	200	102.8	6.38	9.27
6	209	107.6	9.12	12.2
MR-33-1	114	58.7	1.84	1.80
2	128	66.0	2.95	2.90
3	150	77.0	4.10	4.85
4	166	85.3	5.48	7.98
5	177	91.2	7.22	10.3
MR-34-1	75.3	38.8	4.49	2.12
2	82.3	42.3	5.64	3.91
3	88.2	45.4	6.84	5.24
4	101	51.9	9.65	7.91
5	113	58.3	12.6	9.65
6	123	63.0	15.3	12.4
MR-34-7	131	67.1	17.9	14.8
8	139	71.4	13.5	18.3
MR-41-1	132	101	5.87	4.09
2	145	110	6.59	4.51
3	156	118	10.4	11.9
4	160	121	13.4	14.7
MR-42-1	131	99.9	6.18	3.82
2	141	107	7.97	7.50
3	151	114	10.51	9.82
4	156	118	13.2	13.5
5	157	119	13.9	17.0
MR-43-1	95.6	72.6	4.10	2.49
2	106	80.1	4.99	4.17
3	117	88.8	6.38	7.11
4	127	96.8	9.29	9.17
5	132	100	10.8	13.5
6	138	105	11.7	15.3
7	141	107	13.8	19.5
MR-44-1	86.6	65.7	7.69	5.76
2	97.2	73.9	9.77	7.81
3	108	82.1	12.8	10.7
4	115	87.0	14.9	13.7
5	120	91.4	18.2	17.5
6	123	93.4	20.9	21.4

$$\alpha_{LV}=a\Delta H/H_L \tag{9}$$

where

H_L : effective height of riser

ΔH : increase of mercury level

a : ratio of cross sectional areas of separation tank and riser

As the free surface of mercury in the separation tank fluctuated by bubbling, the piping to the level gauge was restricted to damp the fluctuation of the level gauge and to make the measurement easy. The average void fraction obtained in this way was converted into the local void fraction at the point of the flowmeter (II) under the following assumptions.

(1) Linear pressure distribution along the riser.

(2) Constant slip ratio along the riser.

(3) Isothermal condition.

The void fractions measured by th electromagnetic flowmeters were compared with the void fractions calculated from the increase of the liquid level as shown in **Fig. 15**.

Both coincide well. Some tendencies are found from **Fig. 15**; the scatter of data is larger for smaller riser pipes or smaller void fractions, because the level increase is smaller or $K(E_I/E_{II})$ in Eq. 8 approaches 1.0. Then the accuracies of the void fraction measurements by both methods are lowered.

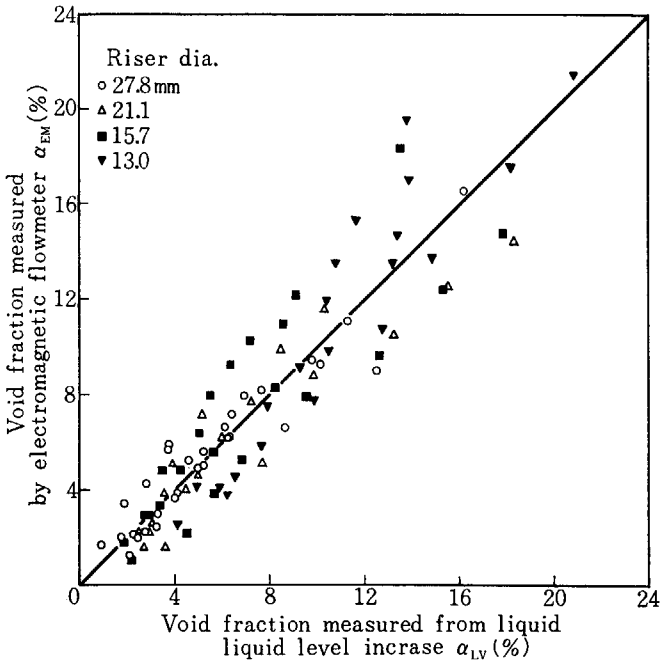

Fig. 15 Results of calibration experiment with real void

4. Feasibility studies with water

4. 1 Simulated void calibration

Calibration experiments using water as the continuous phase were made with simulated voids of acrylic resin rods in order to investigate the effects of void patterns and the orientations of the voids to the electrodes.

A schematic diagram of the calibration apparatus is shown in **Fig. 16**. Water flowed

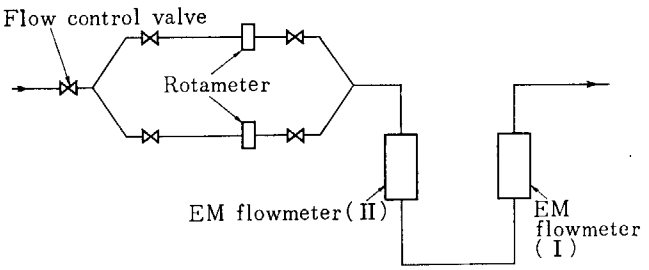

Fig. 16 Schematic diagram of apparatus for simulated void calibration

through the two flowmeters which were set in series. Simulated voids were inserted into the flowmeter (II) for the calibration experiment.

The alternating-current type electromagnetic flowmeters were used for measuring water velocities. The specifications of the two flowmeters used are the same, as follows :

Type : MEP-01 (made by Yokogawa Electric Works, Tokyo, Japan)

Range : 0～10 m/sec

Accuracy : ±1%

Pipe diameter : 25 mm

Pipe length : 500 mm

Inner lining : Teflon

Electrodes : Type 304 stainless steel

The electrical circuit of the flowmeters is shown in **Fig. 17**. The outputs of the pre-amplifiers are recorded by a potentiometer-type mV-recorder.

The patterns, dimensions and void fractions of the simulated voids which were made of acrylic resin are shown in **Fig. 18** and TABLE 6. These simulated voids were inserted into the electromagnetic flowmeter (II), as shown in **Fig. 19**. In the one rod pattern, the rod position was changed in three ways ; center of the pipe, near an electrode and near the side wall. For multi-rod voids the effect of orientation was investigated. City water flowed through the two flowmeters in series. The flow rate was changed from 70 to 700 cm^3/sec, i. e. from 0. 15 to 1. 5 m/sec as the superficial velocity.

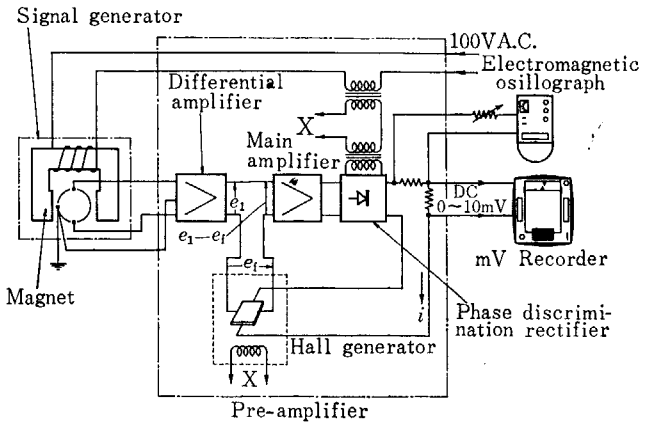

Fig. 17 Electrical circuit of the EM flowmeter

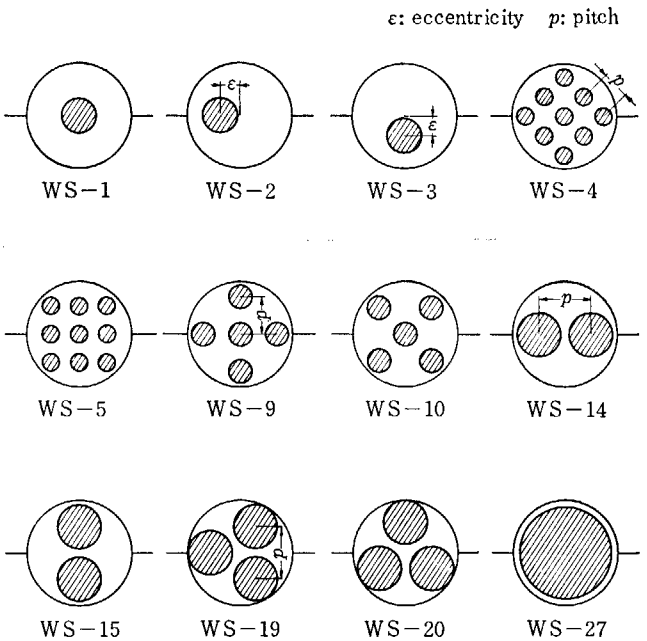

Fig. 18 Simulated void patterns

First, the outputs of the two flowmeters were measured for the same water flow rate. Two flowmeters were used with the same nominal specifications, but the outputs were slightly different. The ratio of the outputs E_I/E_{II} for the same flow rate was 0. 985. Therefore, the void fractions were obtained from Eq. 10.

$$\alpha_{EM}=1-0.985(E_I/E_{II}) \tag{10}$$

Then the simulated voids were placed in the flowmeter (II) and the water was circulated

TABLE 6 Dimensions of Simulated voids

Void No.	Dia. of Rod d (mm)	Number of Rod N (−)	Pitch p (mm)	Eccentricity ε (mm)	Void Area A_V (cm²)	Void Fraction α_{CR} (%)
WS- 1	7.95	1	——	0	0.496	10.7
WS- 2	7.95	1	——	4.32*	0.496	10.7
WS- 3	7.95	1	——	4.32**	0.496	10.7
WS- 4	3.80	9	6.3	——	0.865	18.7
WS- 5	3.80	9	6.3	——	0.865	18.7
WS- 6	11.20	1	——	0	0.984	21.3
WS- 7	11.20	1	——	3.20*	0.984	21.3
WS- 8	11.20	1	——	3.20**	0.984	21.3
WS- 9	5.00	5	8.5	——	0.989	21.4
WS-10	5.00	5	8.5	——	0.989	21.4
WS-11	13.75	1	——	0	1.484	32.1
WS-12	13.75	1	——	2.92*	1.484	32.1
WS-13	13.75	1	——	2.92**	1.484	32.1
WS-14	10.00	2	11.80	——	1.570	33.9
WS-15	10.00	2	11.80	——	1.570	33.9
WS-16	15.90	1	——	0	1.984	42.9
WS-17	15.90	1	——	1.15*	1.984	42.9
WS-18	15.90	1	——	1.15**	1.984	42.9
WS-19	10.00	3	12.0	——	2.360	51.0
WS-20	10.00	3	12.0	——	2.360	51.0
WS-21	18.90	1	——	0	2.543	55.0
WS-22	18.90	1	——	3.10*	2.543	55.0
WS-23	18.90	1	——	3.10**	2.543	55.0
WS-24	19.45	1	——	0	2.970	64.2
WS-25	19.45	1	——	1.17*	2.970	64.2
WS-26	19.45	1	——	1.17**	2.970	64.2
WS-27	21.00	1	——	0	3.462	74.8
WS-28	21.00	1	——	0.60*	3.462	74.8
WS-29	21.00	1	——	0.60**	3.462	74.8

* Eccentric position near an electrode

** Eccentic position near side wall

through the two flowmeters. The diameter and cross-sectional area of the flowmeter (II) pipe were 24.8 mm and 4.63 cm², respectively. In TABLE 7 and **Fig. 21** are compared the void fractions obtained from Eq. 10 using the output of two flowmeters with those calculated from the cross-sectional area of the simulated voids. The measured void fractions, α_{EM}, of TABLE 7 and of **Fig. 21** were the average value of the eight runs for various flow rates. The effect of the flow rate on α_{EM} was not recognized as in the case of mercury.

The void fraction obtained by the electromagnetic method was slightly lower than the value obtained from the cross section of simulated voids. But the effects of the pattern and the orientation were thought to be small.

4.2 Air-water calibration

The calibration experiment using the air-water atmospheric loop was conducted after the simulated void calibration. A schematic diagram of the experimental apparatus for the calibration in the air-water two-phase flow is shown in **Fig. 20**. Water was circulated near the atmospheric

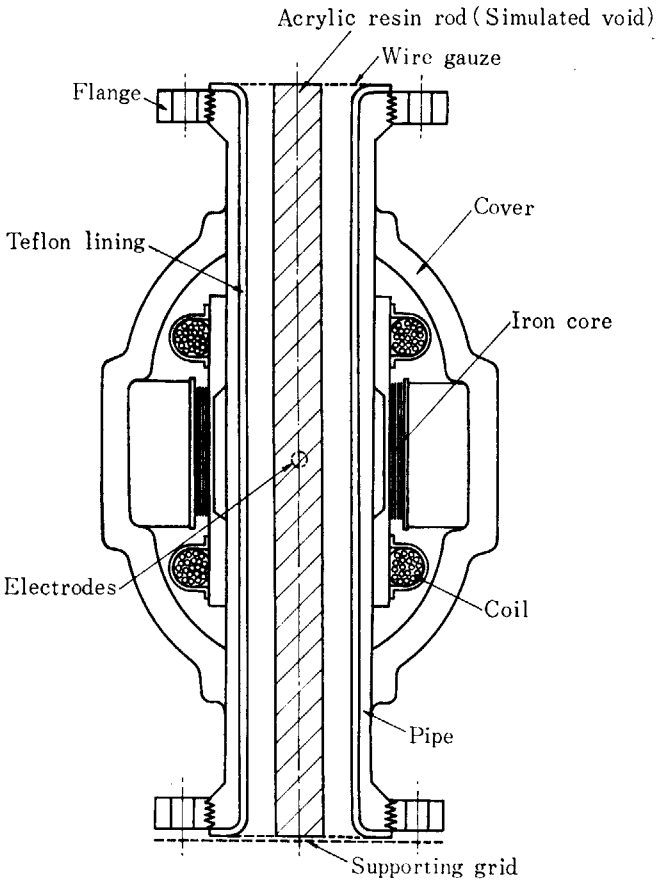

Fig. 19 Simulated void in the EM flowmeter

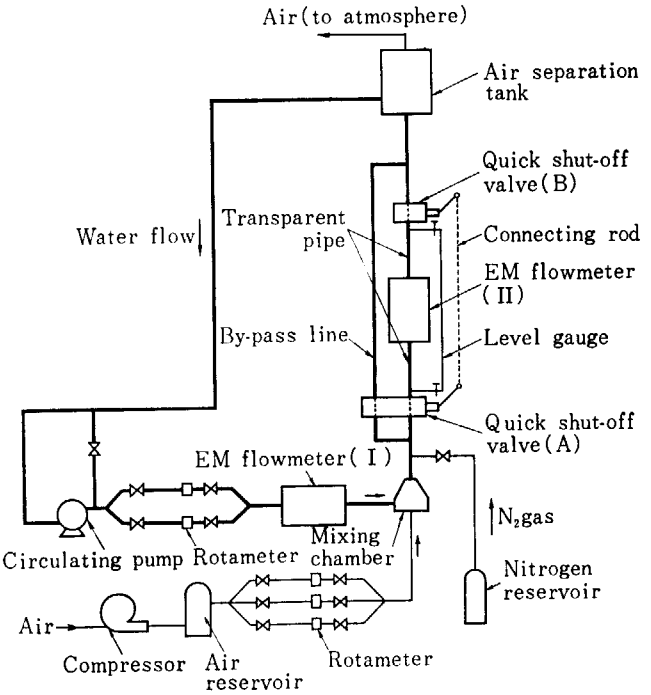

Fig. 20 Schematic diagram of apparatus for air-water calibration

pressure by a centrifugal pump. An electromagnetic flowmeter was placed before the mixing chamber, and the velocity of water flowing in single phase was measured. Air from the compressor was bubbled into water in the mixing chamber, and the flow became two-phase flow. Anothere electromagnetic flowmeter was placed between the two quick shut-off valves in the riser

TABLE 7 Results of simulated void calibration

Void No.	α_{EM} [%]	α_{CR} [%]	Void No.	α_{EM} [%]	α_{CR} [%]
WS- 1	9. 9	10. 7	WS-16	40. 3	42. 9
WS- 2	7. 5	10. 7	WS-17	38. 9	42. 9
WS- 3	8. 9	10. 7	WS-18	41. 0	42. 9
WS- 4	16. 9	18. 7	WS-19	45. 3	51. 0
WS- 5	17. 0	18. 7	WS-20	45. 2	51. 0
WS- 6	17. 6	21. 3	WS-21	50. 7	55. 0
WS- 7	18. 4	21. 3	WS-22	51. 5	55. 0
WS- 8	19. 5	21. 3	WS-23	53. 5	55. 0
WS- 9	20. 3	21. 4	WS-24	60. 3	64. 2
WS-10	17. 2	21. 4	WS-25	61. 0	64. 2
WS-11	30. 1	32. 1	WS-26	61. 0	64. 2
WS-12	27. 2	32. 1	WS-27	71. 0	74. 8
WS-13	29. 9	32. 1	WS-28	72. 1	74. 8
WS-14	31. 0	33. 9	WS-29	71. 7	74. 8
WS-15	27. 8	33. 9			

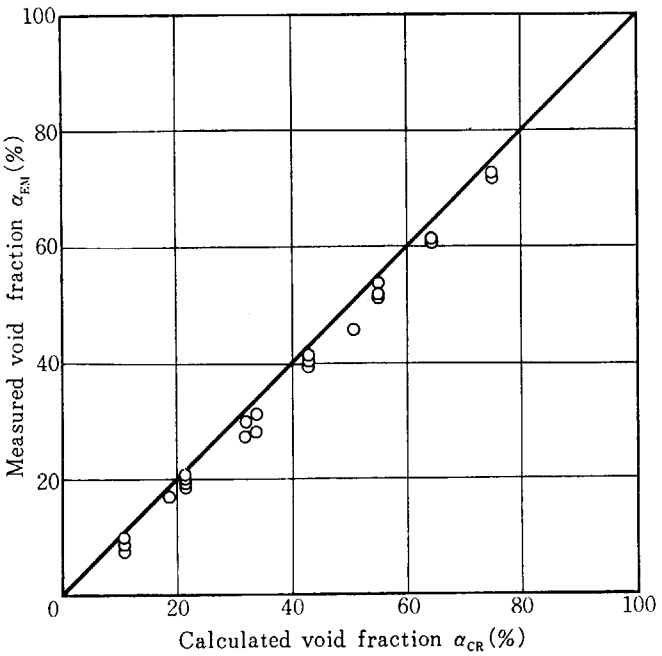

Fig. 21 Results of simulated void calibrations (water)

where the flow was in two-phase. By turning off the valves quickly, and simultaneously, the two-phase flow was confined between the two valves in the riser.

To make a two-phase flow of low void fraction, nitrogen gas from a pressurized nitrogen reservoir was injected through a narrow nozzle. The outline of the quick shut-off valves is shown in **Fig. 22**. The lower valve is double-chambered for by-passing the flow to the air separator while the main line is shut. As the handles of the two valves were connected by the connecting rod, the two valves could be shut off simultaneously and instantaneously by pulling down the rod manually. The time for shutting off the valves was measured for water (single phase) flow velocity of the electromagnetic flowmeter (II) between the two valves.

One example of the oscillograph recordings is shown in **Fig. 23**. The average time for stopping the flow was about 0. 1 sec. The effect of the flow velocity transient of 0. 1 second order was considered to be negligible for measuring void fractions by the quick shut-off method.

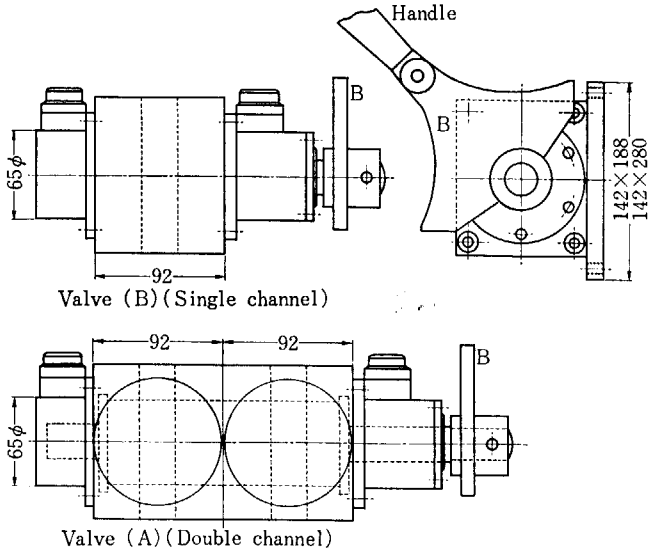

Fig. 22 Quick shut-off valve

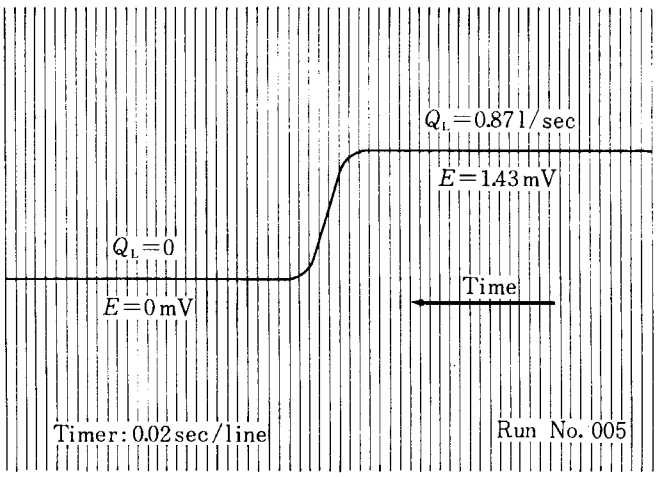

Fig. 23 Output of flowmeter (II) at the moment of shutting the valves

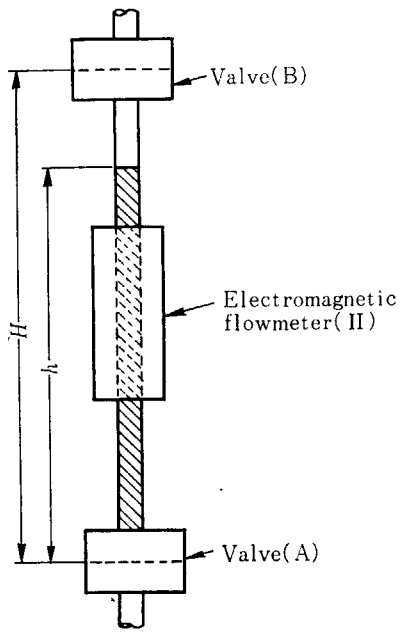

Fig. 24 Water level in the test section (The level is directly visible)

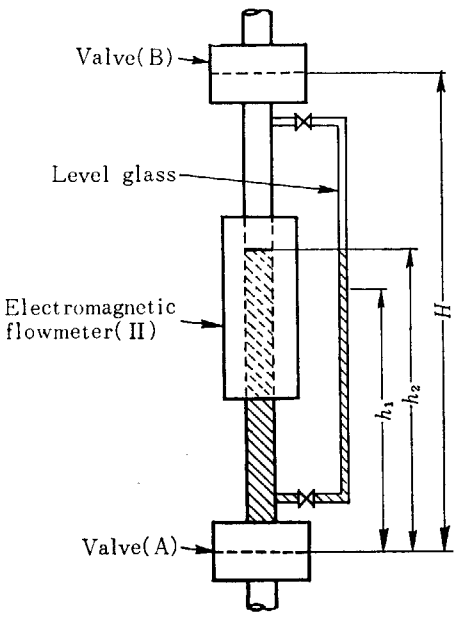

Fig. 25 Water level in the test section (The level is not visible directly)

TABLE 8 Calibration results by quick shut-off method

Run No. 1101～1610 Air-water calibration
Run No. 2201～2609 Nitrogen-water calibration
Run No. 3101～3808 Air-water calibration
Q_L : Water flowrate ($= Q_l$)
α_{QS} : Void fraction obtained by quick shut-off method
α_{EM} : Void fraction obtained by electromagnetic method

Run No.	Q_L [l/sec]	α_{QS} [%]	α_{EM} [%]	Run No.	Q_L [l/sec]	α_{QS} [%]	α_{EM} [%]
WR-1101	0.3	69.5	58.3	WR-2201	0.5	6.4	5.0
1102	〃	65.6	51.4	2202	〃	12.4	10.1
WR-1201	0.5	60.6	53.9	2203	〃	18.4	13.7
1202	〃	58.7	52.0	2204	〃	22.8	16.2
1203	〃	52.0	46.7	2205	〃	28.3	21.6
1204	〃	47.2	44.6	2206	〃	28.3	20.6
1205	〃	34.6	36.9	2207	〃	23.8	20.0
1206	〃	31.9	34.4	2208	〃	19.4	15.7
1207	〃	43.5	42.4	2209	〃	13.8	12.3
1208	〃	54.7	47.0	2210	〃	6.5	5.1
1209	〃	56.4	51.7	WR-2301	0.8	6.7	5.3
1210	〃	61.1	55.5	2302	〃	11.8	10.4
WR-1301	0.8	63.8	52.7	2303	〃	16.1	15.2
1302	〃	57.7	48.7	2304	〃	16.3	19.3
1303	〃	49.6	43.1	2305	〃	27.2	29.2
1304	〃	34.6	36.6	2306	〃	26.1	29.2
1305	〃	22.2	25.7	2307	〃	22.7	22.2
1306	〃	24.8	27.7	2308	〃	16.8	14.6
1307	〃	33.6	——	2309	〃	12.1	8.7
1308	〃	50.9	43.5	2310	〃	6.7	6.7
1309	〃	57.3	48.2	2311	〃	11.7	9.9
1310	〃	66.9	53.5	WR-2501	1.0	11.0	12.2
WR-1501	1.0	57.1	51.4	2502	〃	18.5	19.9
1502	〃	51.2	47.1	2503	〃	26.5	26.2
1503	〃	48.2	42.3	2504	〃	30.1	27.6
1504	〃	34.1	34.2	2505	〃	29.4	28.4
1505	〃	21.7	22.8	2506	〃	28.0	26.9
1506	〃	20.0	22.0	2507	〃	18.0	19.2
1507	〃	33.3	33.1	2508	〃	7.3	8.4
1508	〃	42.6	41.6	2509	〃	7.4	8.4
1509	〃	54.5	48.3	WR-2601	1.2	11.3	10.4
1510	〃	65.1	52.5	2602	〃	14.5	21.8
WR-1601	1.2	59.3	52.0	2603	〃	21.7	26.7
1602	〃	49.8	47.2	2604	〃	——	——
1603	〃	44.2	32.4	2605	〃	32.1	29.2
1604	〃	31.1	30.8	2606	〃	32.2	29.2
1605	〃	19.1	20.8	2607	〃	27.3	26.9
1606	〃	20.3	21.2	2608	〃	21.6	21.4
1607	〃	32.5	31.8	2609	〃	11.6	12.0
1608	〃	47.8	42.4	WR-3101	0.3	89.4	79.7
1609	〃	54.1	47.6	3102	〃	85.9	77.8
1610	〃	59.2	52.1	3103	〃	83.6	72.8

TABLE 8 (Continued)

Run No.	Q_L [l/sec]	α_{QS} [%]	α_{EM} [%]	Run No.	Q_L [l/sec]	α_{QS} [%]	α_{EM} [%]
WR-3104	0.3	81.5	66.0	WR-3707	0.1	89.4	86.0
3105	〃	80.4	67.5	3708	〃	93.4	86.1
3106	〃	83.3	72.6	3709	〃	93.7	86.1
3107	〃	85.7	78.0	3710	〃	93.2	86.0
3108	〃	90.5	79.1	WR-3801	0.2	92.5	81.7
3109	〃	79.9	72.3	3802	〃	89.6	80.5
WR-3701	0.1	89.9	83.5	3803	〃	83.8	76.4
3702	〃	85.7	76.2	3804	〃	——	67.3
3703	〃	84.2	74.3	3805	〃	81.8	78.5
3704	〃	81.0	74.7	3806	〃	82.8	76.4
3705	〃	81.6	74.7	3807	〃	90.9	80.5
3706	〃	85.2	76.6	3808	〃	92.4	80.3

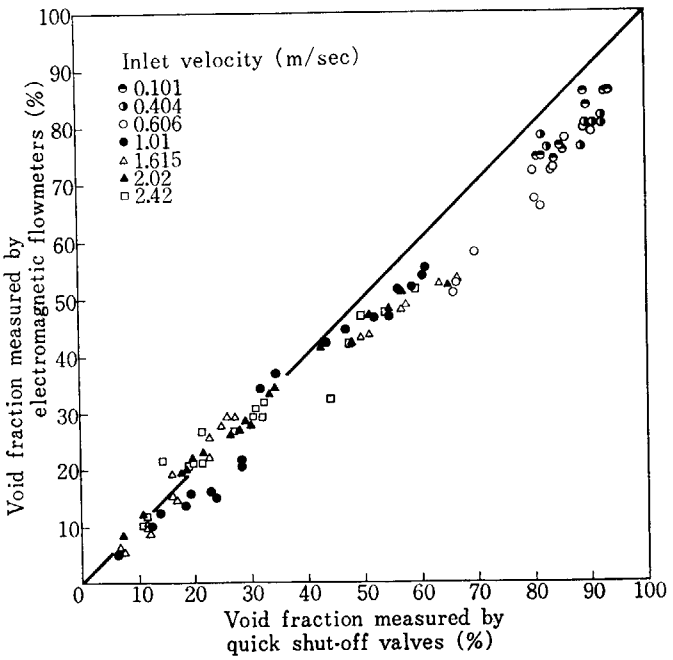

Fig. 26 Calbration results by air-water two-phase flow

The length of the test section, i. e., the distance between two valves, was 1430 mm, and the inside diameter of the test section was 25 mm. The electromagnetic flowmeter was placed at the middle of the test section. The flowmeter and the valves were connected by transparent pipe of acrylic resin.

The method for obtaining the void fraction by quick shut-off valves is as follows:

(1) When the water level is visible (**Fig. 24**), the average void fraction in the test section, α_{QS}, can be obtained from

$$\alpha_{QS}=1-\frac{h}{H} \tag{11}$$

where

H: height of the test section

h : height of the water level

(2) When the water level is not visible directly (**Fig. 25**), by introducting the water into the level gauge, the average void fraction in the test section, α_{QS}, can be obtained from

$$\alpha_{QS}=1-\frac{h}{H} \tag{12}$$

$$h=h_2+(d/D)^2(h_2-h_1) \tag{13}$$

where

D : inside diameter of the test section

d : inside diameter of the level gauge

h_1 : height of the water level gauge before introducing water into the gauge

h_2 : height of the water level gauge after introducing water into the gauge

Two flowmeters used were the same as those used for the simulated calibration experiment. The outputs of the two electromagnetic flowmeters were measured by the mV recorder and the oscillograph of which electrical connections are shown in **Fig. 17**. To give the sufficient electrical conductivity to the water, copper sulphate was added to city water, the conductivity then becoming $40\sim100\,\mu\mho$/cm. The flow rate of water was changed as follows:

Q_L(1/sec)	0.1	0.2	0.3	0.5	0.8	1.0	1.2
V_{IIS}(m/sec)	0.202	0.404	0.606	1.01	1.62	2.02	2.42

Where V_{IIS} is the superficial velocity of water in the test section. The air (or nitrogen) flow rate was changed up to 22.3 1/sec to provide various void fractions.

The void fraction obtained from the electromotive forces of the two flowmeters was comparad with those obtained by the quick shut-off method (TABLE 8 and **Fig. 26**). The mV outputs measured by the mV-recorder were used for obtaining α_{EM} of the TABLE 8 and **Fig. 26**. The coincidence between α_{EM} and α_{QS} is fairly well at comparatively low void fractions. However, the outputs of the flowmeter in the test section became oscillatory, due to the oscillatory flow pattern of the two-phase flow in high void fraction. In this case, the time average value of the oscillatory electromotive force was used for the void calculation. As will be seen from **Fig. 26**, the void fractions obtained by the electromagnetic method are smaller than those obtained by the quick shut-off method for high void fractions (above 40%). This discrepancy will be discussed in Chapter 5.

Examples of oscillographs are shown in **Fig. 27**. As seen from these recordings, the outputs of flowmeter (II) become oscillatory as the void fraction increases. In **Fig. 27**(1) is shown the case of bubble flow ($\alpha_{QS}=11\%$). In the bubble flow, the velocity of liquid phase and void fraction are constant and the output E_{II} is stable. As the air flow rate was incrased, the output of the flowmeter (II) became oscillatory because the flow pattern changes from the bubble flow to the slug flow (**Fig. 27**(2)$\sim$(3)).

In the slug flow, the liquid-phase velocity changes because the gas phase flows in lumps and the void fraction changes longitudinally in the test section.

Fig. 27 (6) and (7) show the cases of low water flow rate with high void fractions (82% and 93%). In the high void fraction, the output E_{II} tend to become less oscillatory as the void fraction increases. This is due to the fact that the flow pattern changes from slug flow to slug-annular flow. It is estimated that in annular flow the output of the flowmeter becomes stable because the liquid-phase flows steadily along the wall. But this was not confirmed because no annular flow was observed in this experiment.

In oscillatory flow patterns such as slug flow, the water flow rate, which is measured by the electromagnetic flowmeter (I) in the single-phase region, becomes also oscillatory. This is probably because the slug flow accompanies the pressure oscillation and this oscillation in the mixing chamber makes change in the feed rate of water and air to the test section. Therefore

(1) Run No : WR-2501
Q_L : 1.0l/sec
α_{QS} : 11.0%
α_{EM} : 12.2%

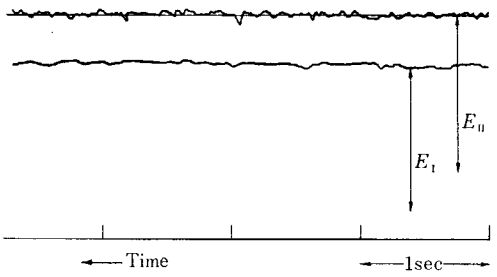

(2) Run No : WR-2502
Q_L : 1.0l/sec
α_{QS} : 18.5%
α_{EM} : 19.9%

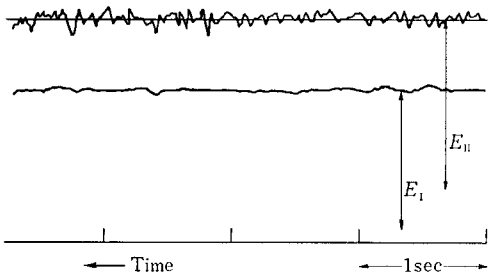

(3) Run No : WR-1507
Q_L : 1.0l/sec
α_{QS} : 33.3%
α_{EM} : 33.1%

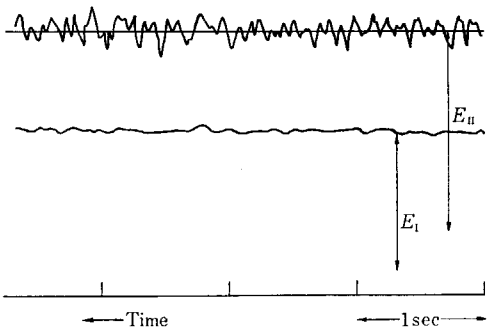

(4) Run No : WR-1503
Q_L : 1.0l/sec
α_{QS} : 48.2%
α_{EM} : 42.3%

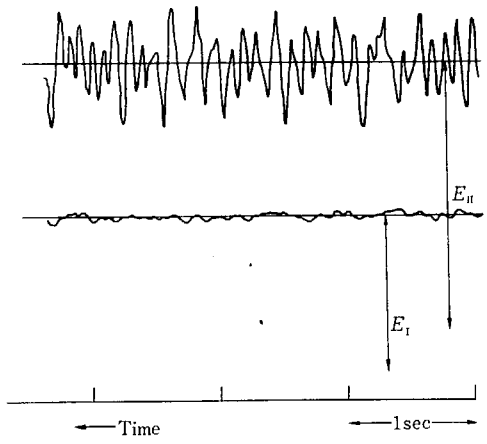

(5) Run No : WR-1510
Q_L : 1.0l/sec
α_{QS} : 65.1%
α_{EM} : 52.5%

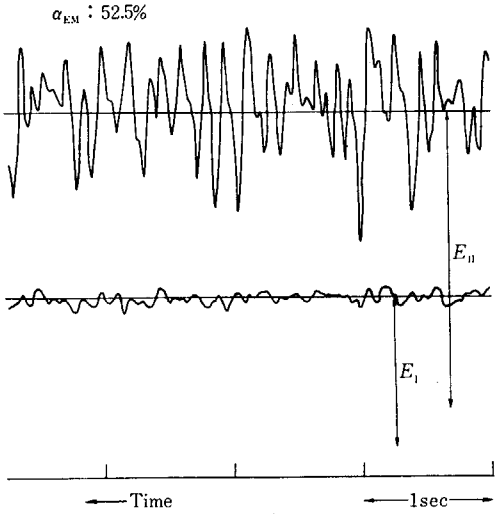

(6) Run No : WR-3805
Q_L : 1.0l/sec
α_{QS} : 81.8%
α_{EM} : 78.5%

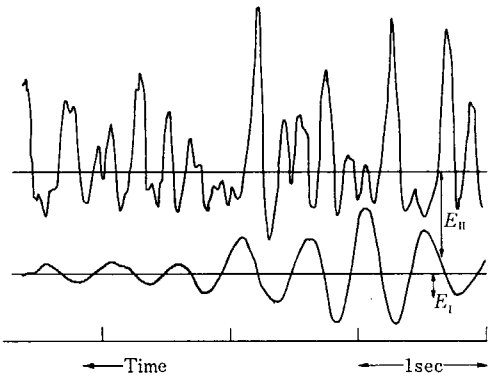

(7) Run No: WR-3801
Q_L : 0.2% l/sec
α_{QS} : 92.5%
α_{EM} : 81.7%

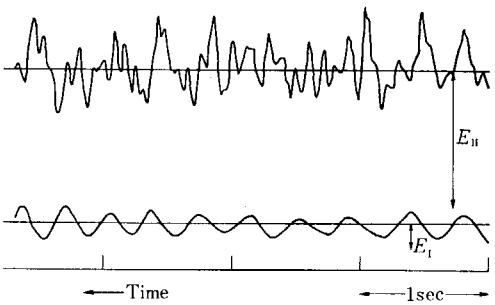

Fig. 27 EM flowmeter output recordings on the oscillograph
Q_1 : Water flow rate (1/sec)
α_{QS} : Void fraction measured by the quick shut-off valves (%)
α_{EM} : Void fraction measured by the EM flowmeters (%)

the system characteristics, such as that of the circulating pump or compresser, the resistance and capacitance in the pipings, is considered to exert great influence on the two-phase flow pattern.

In the air-water flow, the cut-off of the electromotive force due to the covering of the electrodes with an air bubble was not observed, probably because of the good wettability of water to the electrode material (stainless steel).

5. Discussion

5. 1 Effect of flow oscillation

When the void fraction varies with time as in the case of slug flow, observing the flow at a certain section, the average void fraction $\bar{\alpha}$ should be defined

$$\bar{\alpha}=\frac{\int \alpha dt}{\int dt} \tag{14}$$

This average void fraction is equal to that obtained by the quick shut-off method, when the integral is made for a sufficiently long time and the length between the quick shut-off valves is long enough compared with the length of the gas lump. As described in Chapter 2, the electromagnetic method using Eq. 4 is applicable only when the liquid flow rates at the flowmeters (I) and (II) are the same, that is $Q_{\mathrm{I}}=Q_{\mathrm{II}}$. In slug flow this condition does not always hold because the flow is not homogeneous and large lumps of gas flow faster than the liquid-phase. In spite of this fact, if the equation such as the Eq. 5 could be used in slug flow using the time average velocity $\overline{V}_{\mathrm{II}}$ instead of V_{II}, the eqation will be expressed as follows;

$$\bar{\alpha}=1-\frac{V_{\mathrm{I}}}{\overline{V}_{\mathrm{II}}} \tag{15}$$

Then the time average velocity $\overline{V}_{\mathrm{II}}$ is derived from Eq. 14 and 15.

$$\overline{V}_{\mathrm{II}}=\frac{V_{\mathrm{I}}}{\left(1-\frac{\int \alpha dt}{\int dt}\right)}=\frac{\int V_{\mathrm{II}}(1-\alpha)dt}{\int (1-\alpha)dt} \tag{16}$$

where V_{I} is constant.

Eq. 16 has the unknown factor α, so $\overline{V}_{\mathrm{II}}$ can not be calculated from the flowmeter output. The average value which used for the calculation of $\bar{\alpha}$ in Chapter 4, $\overline{V}'_{\mathrm{II}}$, is expressed by Eq. 17.

$$\overline{V}'_{\mathrm{II}}=\frac{\int V_{\mathrm{II}}\,dt}{\int dt} \tag{17}$$

The average value defined by Eq. 17 is obtained graphically from the output recordings as shown in **Fig. 28**, of which the upper and lower shaded areas are equal.

In the case of bubble flow, the avrage values $\overline{V}_{\mathrm{II}}$ and $\overline{V}'_{\mathrm{II}}$ are almost the same. But in the slug flow, the output of flowmeter (II) oscillate violently and $\overline{V}_{\mathrm{II}}$ and $\overline{V}'_{\mathrm{II}}$ do not coincide. As shown in **Fig. 29** the gas-phase flows faster than the liquid-phase and slip between both phases occur in the section where the gas-phase flows in a lump, then the upward liquid velocity

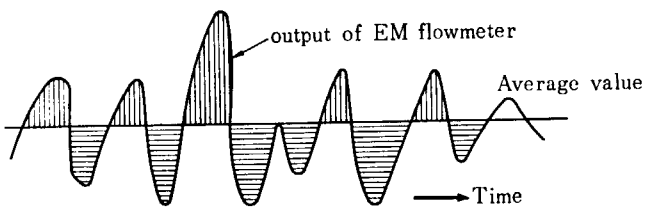

Fig. 28 Average void fraction defined by Eq. 17

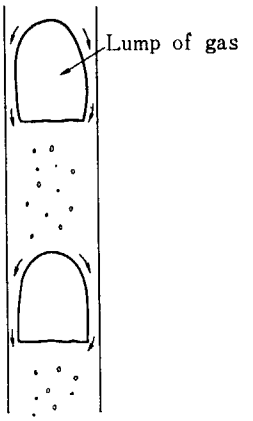

Fig. 29 Flow pattern of slug flow

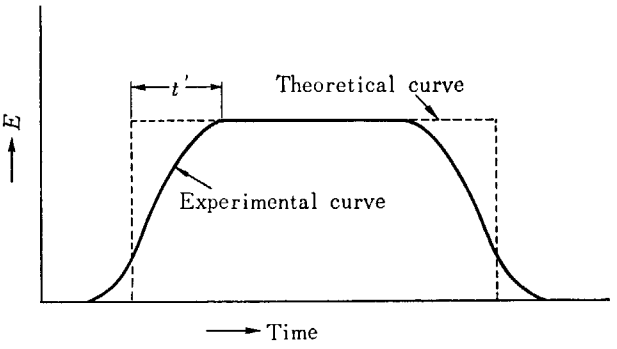

Fig. 31 Output of EM flowmeter

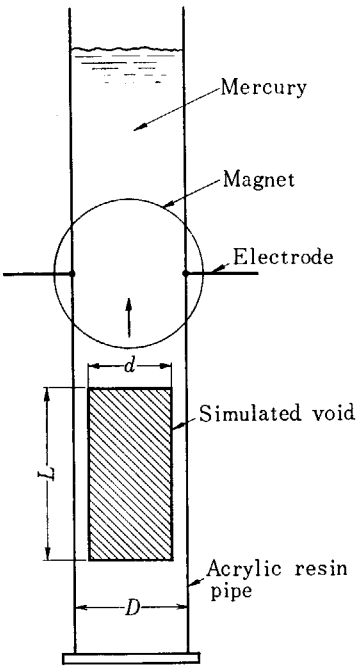

Fig. 30 Experiment with simulated slug

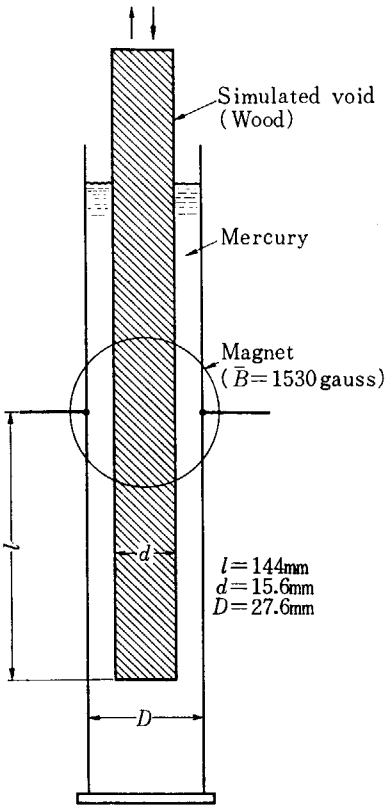

Fig. 32 Experiment for end-shunt effect

decreases. In the extreme cases, the liquid flows downward in spite of the constant feeding of the liquid at the inlet. Therefore the following condition is thought when a slug flow is observed at a certain section :

At the moment when the void fraction is high, the mean velocity of liquid-phase is low.

At the moment when the void fraction is low, the mean velocity of liquid-phase is high.

Comparing the two average values $\overline{V}_{II}$ and $\overline{V}'_{II}$ with the above condition for slug flow, following equation will be derived.

$$\overline{V}_{II} > \overline{V}'_{II} \tag{18}$$

That is, the average value obtained from Eq. 17 is lower than that from Eq. 16. As Eq. 16 gives a correct value, the void fraction obtained from Eq. 17 should become lower than the real value. As α_{EM} of **Fig. 26** and **TABLE 8** were obtained using $\overline{V}'_{II}$, it is natural that α_{EM} became lower than α_{QS} for the high void fraction in which case the two-phase flow became oscillatory.

In conclusion, the electromagnetic method gives the correct void fraction by Eq. 4 only

when the two-phase flow pattern is non-oscillatory, i. e. bubble-flow or annular-flow. It can be examined whether the void fraction obtained by the electromagnetic method is correct or not from the amplitude of the output oscillation. The correct time average velocity which is obtained from Eq. 16 should be between the maximum velocity and $\overline{V}'_{II}$ by Eq. 17. Therfore, if the difference between maximum velocity and $\overline{V}_{II}$ is small, the error of α_{EM} is concidered to be small. By recording the flowmeter output using an oscillograph, the error of α_{EM} and the applicability of this method are estimated.

In the above discussion, the output (electromotive force) of the electromagnetic flowmeter is assumed to be proportional to the mean velocity of the liquid. When the liquid velocity changes in the direction flow, as in the slug flow, however, the output is somewhat different from the value corresponding to the real velocity, because of the end-shunt effect at the edge of the gas slug.

This effect was investigated experimentally and the result is shown in the following.

In the slug flow, the liquid of annulus around the gas slug flows slower than the liquid portion between the slugs, because the velocity of the gas slug is greater than that of the liquid phase, and the slip exists between two-phase. The actual two-phase slug flow can be simplified to the case as shown in **Fig. 30**. Subtracting the superficial liquid velocity from the flow system, then the actual flow is considered to be equivalent to the case that the gas slug is rising through the stagnant liquid.

For studying such a simplified case, a simulated slug made of acrylic resin was moved up from the bottom of the pipe and the outputs of the electromagnetic flowmeter were recorded. In this case, the average downward velocity of liquid annulus is denoted by V_1, then the output, E, is;

$$E=KBDV_1\times 10^{-5} \tag{19}$$

or integrating by passing time of the slug through the electrode,

$$\int_0^t Edt=KBD\times 10^{-5}\int_0^t V_1 dt=KBD\frac{d^2l}{D^2-d^2}\times 10^{-5} \tag{20}$$

where

E : Output of EM-flowmeter (mV)
K : Constant (—)
B : Magnetic flux density (gauss)
D : Diameter of the pipe and the distance between the electrodes (cm)
d : Diameter of the slug (cm)
l : Length of the slug (cm)
V_1: Average downward velocity of liquid (cm/sec)

The output recorded by an oscillograph was different from the value calculated by Eq. 19 as shown in **Fig. 31** in which the dotted line shows the calculated value. This is due to the end shunt effect at the upper and lower ends of the slug where the liquid velocity changes abruptly. The transient time of the output, t', is corresponding to about 2 cm in length and the pipe inside diameter is 2. 76 cm, so it is concluded that the output does not show the real value untill the slug end passes the electrode by the distance of about two third of the inside diameter of the pipe.

The slug flow was also simulated by moving the simulated slug up and down several times, the lower end reaching the free surface at the highest position and the lower end reaching 144 mm below the electrode at the lowest position, as shown in **Fig. 32**. The variation of the output was recorded in the oscillograph and $\int Edt$ was integrated graphically. The velocity of the

slug was changed and the effect of the slug velocity on the outputs was investigated. The results are as follows;

Average slug velocity (cm/sec)	3. 9	10. 3	13. 9
$\int Edt$ (mV-sec)	0. 245	0. 240	0. 248

The results show that the variation of $\int Edt$ due to the slug velocity is very small and is within the experimental error. There was also no difference in $\int Edt$ for the moving directions, up and down. The experimental value of $\int Edt$ is compared with the calculated value obtained by Eq. 20, then

$$\frac{(\int Edt)_{\text{exp}}}{(\int Edt)_{\text{calc}}} = 0.913 \sim 0.943 \tag{21}$$

The ratio shows quantitatively the effect of the end shunt at the edge of slug. If it is assumed that the average output is a half of the the theoretical while the slug edge is within 2 cm from the electrode, this ratio should be as follows;

$$\frac{(\int Edt)_{\text{exp}}}{(\int Edt)_{\text{calc}}} = \frac{\frac{12.4}{14.4}E + \frac{2.0}{14.4}E \times \frac{1}{2}}{E} = 0.933 \tag{22}$$

This value agrees with that obtained from Eq. 21.

From this experiments described above, it is concluded that the EM flowmeter output is somewhat different from the value corresponding to the real velocity when the liquid velocity changes in the direction of flow. This end shunt effect at the edge of gas slug will increase the error in obtaining the void fraction by Eq. 14 and Eq. 17.

5. 2 Application ot electromagnetic flowmeter to the flow pattern identification

Usually, visual or photographic observations are used for the study of two-phase flow pattern. An application of the EM flowmeter to the two-phase flow pattern study will now be considered. As described in the previous chapters, the output of the EM flowmeter is nearly proportional to the average velocity of liquid-phase. Therefore, the recordings of the flowmeter output indicate the flow pattern.

In bubble flow, the output of the flowmeter is stable, as show in **Figs. 27** (1) and (2). But in slug flow, the void fraction varies with time and output oscillation occurs as shown in **Figs. 27** (3) ~ (7). Thus, when the void fraction in the flowmeter varies with time, the liquid-phase velocity and hence the output of the flowmeter varies with time. Therefore, from the output recordings of the flowmeter, the flow pattern can be estimated. For opaque liquid or opaque wall in which liquid flows, visual observasion is impossible and this method can be considered useful. Also, this method can be used for the quantitative representation of flow pattern which is usually qualitatively defined.

5. 3 Application of the electromagnetic method to complex shaped channels

Calibration experiments were made for the flow in a circular channel. In boiling water reactors, the measurement of void fractions in more complex channels is important. Several methods of the void measurement for such case will be described in the following. **Fig. 33** shows the measuring methods for annular channel, 7-rod cluster channel and 9-rod cluster rectangular channel, using transverse-field type electromagnetic flowmeter.

Fig. 34 shows the application of an axial-current type electromagnetic flowmeter to void measurements. In this case, the electric current flows in parrarel with the fluid flow and the

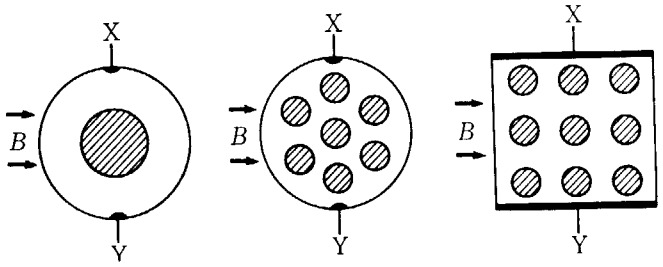

Fig. 33 Void measurements by transverse-field type flowmeter
B : Magnetic flux X, Y : Electrodes

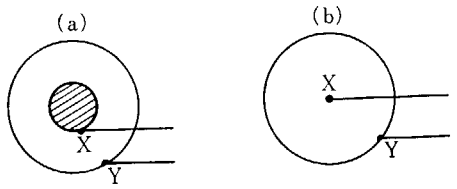

Fig. 34 Void measurements by axial-current type flwmeters
X, Y : Electrodes

electromotive force will be produced radially. In **Fig. 34(a)** the electric current which will make excitation (and heating if desired) flows through the inner rod. The electrodes are set on the rod surface and the channel surface.

The above methods can be applied, not only to two-component two-phase flows such as an air-water system, but also to one-component two-phase flows such as a steam-water system. In both cases the surface of the rods and channel must be electric insulater.

Fig. 34 (b) shows another method which may be applied to liquids with good electric conductivity such as liquid-metal. Electric current flows through the liquid in parralel with the flow, and the electromotive force will be produced between the two electrodes, which are located in the center of the tube and tube wall. The fluid can be heated either from the channel wall or by the electric resistance heating in the fluid itself.

6. Conclusion

Calibration experiments for the present electromagnetic void measurement method were made for circular channels, using argon-mercury and air-water system. Simulated void calibrations were also made for both mercury and water cases.

The results show that this void measurement method can be used in two-phase flows of non-oscillatory flow pattern, i. e. bubble flow, without calibration, and with calibration for oscillatory flow pattern, i. e. slug flow. Annular flow was not observed in the experiments, but this method is also considered to be applicable to this flow pattern.

This method can be applied to more complex shaped channels or to one-component two-phase flow with phase change. The output recordings of the electromagnetic flowmeter in two-phase flow will be useful for estimating and analysis of the flow pattern, especially for the case of opaque liquid.

Acknowledgement

The authors wish to express their thanks to Prof. F. TACHIBANA of Tokyo University and Mr. K. TORIKAI, chief of Heat Transfer Laboratory, for useful discussions. Thanks are also due to Mr. A. KIKUCHI for his cooperation in the experiments.

References

1) M. HORI, T. KOBORI and Y. OUCHI, ; Preprint of 1963 Annual Meeting of Atomic Energy Society of Japan, No. D-25, pp 183 (1963)
2) M. HORI, T. KOBORI, Y. OUCHI and A. KIKUCHI ; Preprint of Meeting on Nuclear Engineering held by Atomic Energy Society of Japan, No. 19, pp 19 (1963)
3) J. A. SHERCLIFF : "The Theory of Electromagnetic Flow Measurement" pp 23～27, Cambridge Press, London (1962)